Acoustic "Re-charging" of Nanofiber Air Filters†

Le Xu, Zhenyu Zhu, Baojun Qiu, Shipeng Hou, Linyi Cui, Hongyuan Wei, Hongxia Wang*, Tong Lin*

[1] School of Textile Science and Engineering, Tiangong University, Tianjin 300387, China
[2] The Key Laboratory of Hollow Fiber Membrane Materials and Membrane Processes, Ministry of Education, Tiangong University, Tianjin 300387, China

*Corresponding Authors' emails: Hongxia Wang, hongxiawang@tiangong.edu.cn; Tong Lin, tong.lin@tiangong.edu.cn

Electronic Supplementary Information

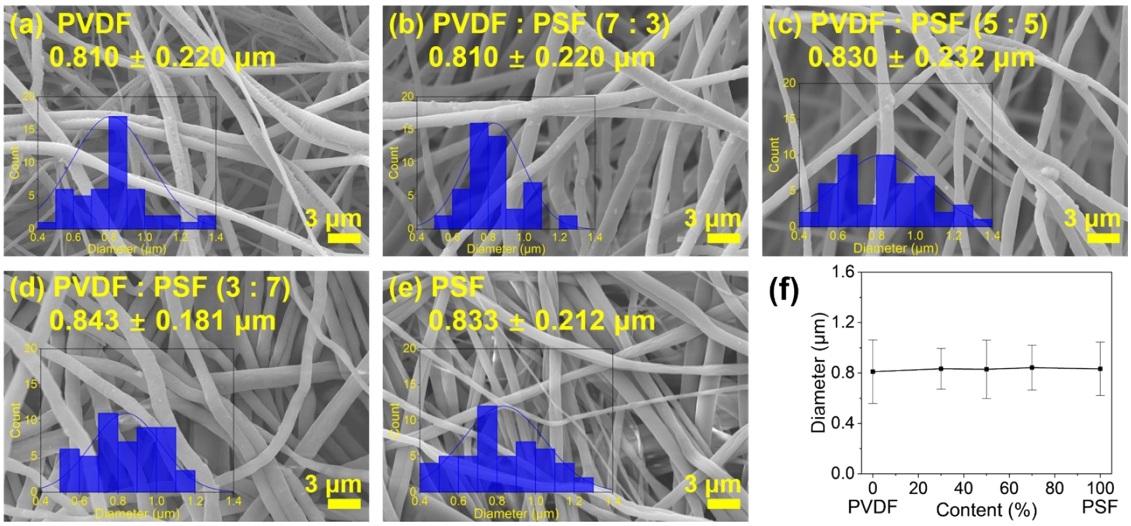

Figure S1. (a-e) SEM images, diameter distributions, and (f) average diameter and diametrical distribution of the nanofibers with different PSF contents prepared from different conditions.

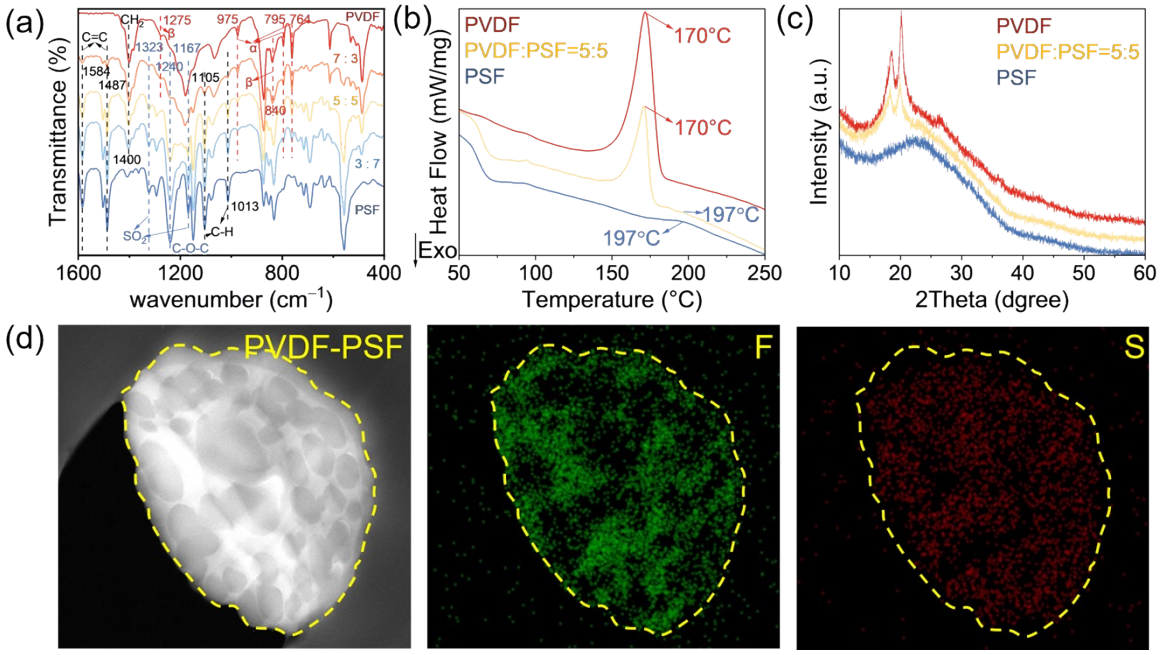

Figure S2. (a) FTIR spectra, (b) DSC curves, and (c) XRD curves of PVDF, PSF, and PVDF-PSF nanofiber membranes. (d) Cross-sectional TEM and TEM-EDS mapping images of elements F and S. (PVDF: PSF=1:1 wt/wt for the PVDF-PSF nanofibers)

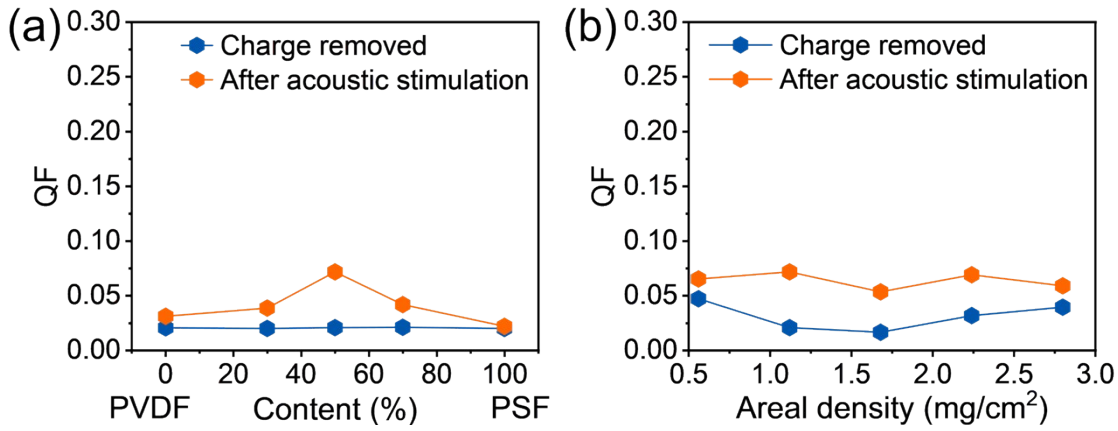

Figure S3. Effects of (a) PSF content and (b) areal density on the QF of PVDF-PSF nanofiber membranes for filtering 0.3 μm NaCl aerosol particles. (airflow rate 32 L/min, fiber diameter 830 nm, areal density 1.12 mg/cm^2 for a; PVDF-PSF=1:1 wt/wt for b)

The influence of membrane thickness, expressed as areal density, on filtration performance is summarized in Figures 1e and 1f. Low areal density membranes (PVDF: PSF = 1:1 wt/wt, 0.56 mg/cm², ~10 μm thickness) exhibited modest baseline performance (η = 64.59%, ΔP = 22 Pa) with only slight acoustic improvement (η = 69.12%, ΔP = 18 Pa). At 1.12 mg/cm² (~30 μm thickness), acoustic stimulation boosted η to 91.89% and reduced ΔP to 35 Pa, yielding a marked QF increase from 0.021 to 0.072 (ΔQF = 0.051, Figure S3). Further increases in areal density (e.g., 2.80 mg/cm²) raised η to 99.99% but caused a disproportionate rise in ΔP (117 Pa), reducing overall QF. This reveals a key trade-off: moderate areal density (1.12–1.68 mg/cm²) balances high filtration efficiency, low airflow resistance, and maximal acoustic responsiveness.

The effect of fiber diameter on filtration performance is illustrated in Figures 1g and 1h. At constant areal density (1.12 mg/cm²), finer fibers (290 nm) achieved near-unity η (99.99%) but at the cost of very high ΔP (250 Pa, baseline QF = 0.037, Figure S5). Coarser fibers (1.18 μm) showed low η (57.05%) and ΔP (33 Pa, baseline QF = 0.026). Under acoustic stimulation, 660 nm fibers exhibited a dramatic QF enhancement from 0.015 to 0.209, with η rising to 99.99% and ΔP falling to 44 Pa. A similar trend was observed for 830 nm fibers, indicating that 660–830 nm is the optimal fiber diameter range for robust acoustoelectrical coupling and balanced filtration performance.

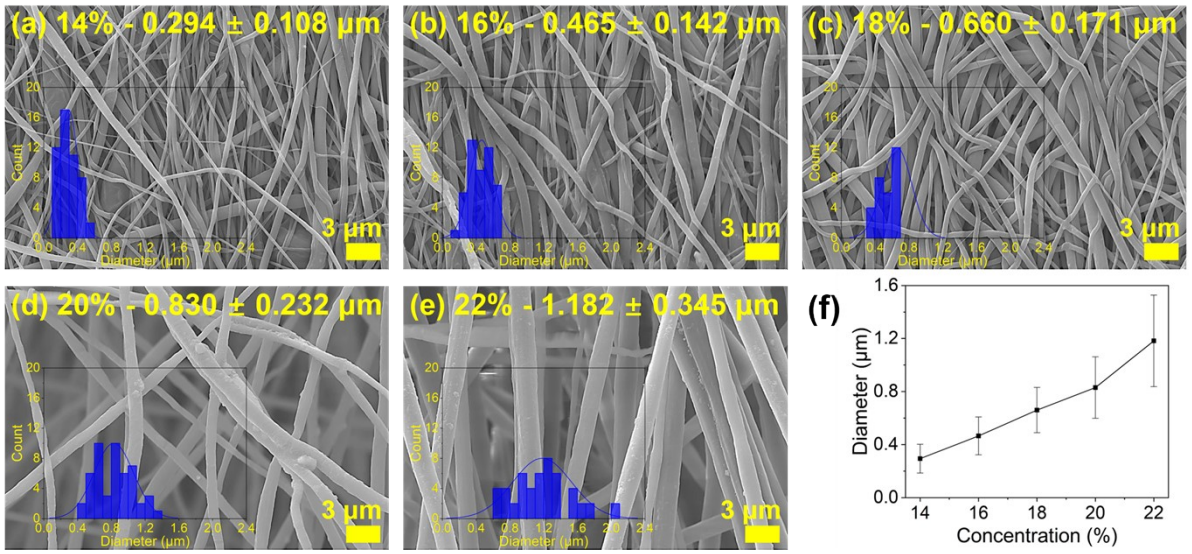

Figure S4. (a-e) SEM images, diameter distributions, and (f) diameters of PVDF-PSF nanofibers electrospun from PVDF-PSF (1:1, wt/wt) with different overall concentrations.

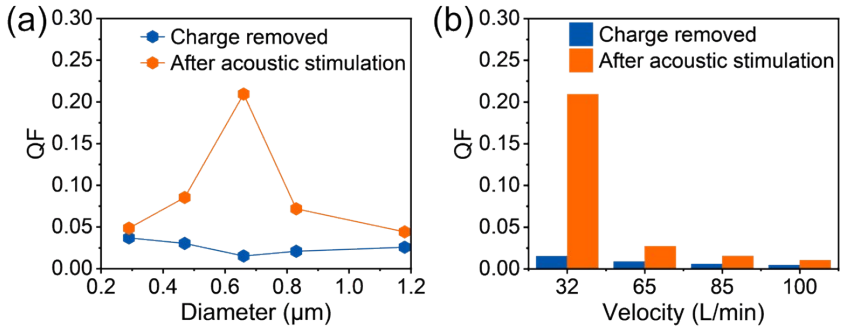

Figure S5. Effects of (a) nanofiber diameter and (b) airflow rate on the QF of the PVDF-PSF nanofiber membranes for $PM_{0.3}$ NaCl. (PVDF: PSF=1:1 wt/wt, areal density of 1.12 mg/cm^2, airflow rate of 32 L/min for a; fiber diameter 660 nm for b)

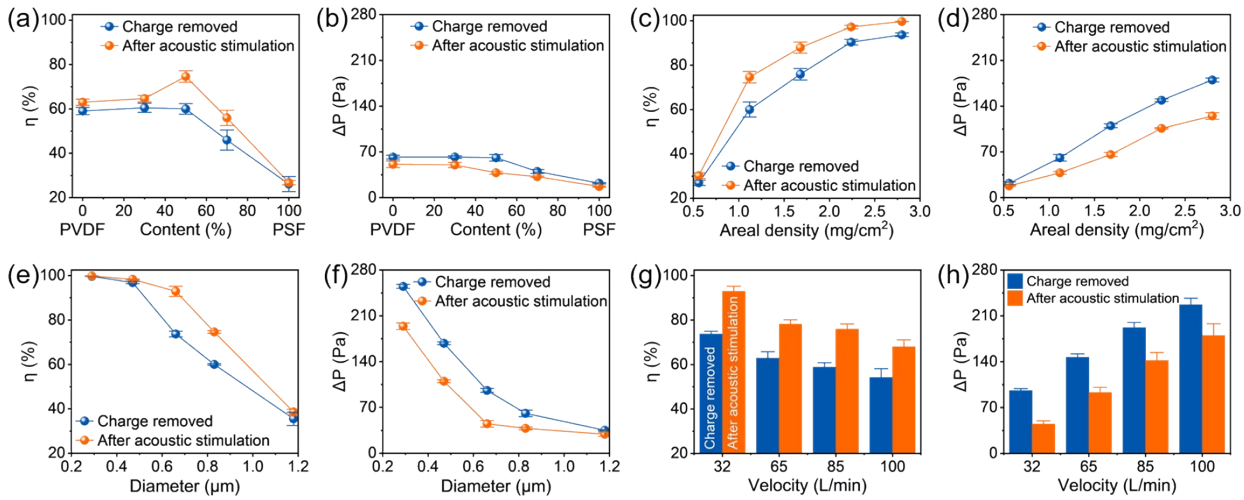

Figure S6. Effects of (a, b) PSF content, (c, d) membrane areal density, (e, f) fiber diameter, and (g, h) airflow rate on η and ΔP of PVDF-PSF nanofiber membranes for $PM_{0.3}$ DEHS. (Airflow rate 32 L/min for a-h, PSF content 50% for c-h, fiber diameter 830 nm for a-d, fiber diameter 660 nm for g-h, areal density 1.12 mg/cm^2 for a-b and e-h, and acoustic regeneration at 100 Hz, 110 dB, 10 minc for a-h)

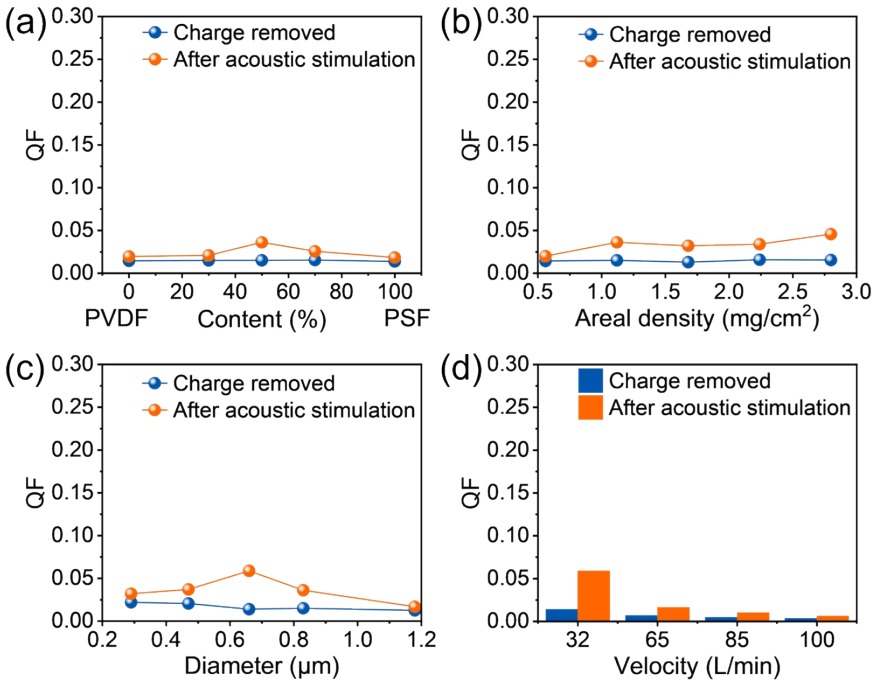

Figure S7. Effects of (a) PSF content, (b) areal density, (c) nanofiber diameter, and (d) airflow rate on the QF of PVDF-PSF nanofiber membranes for $PM_{0.3}$ DEHS. (Airflow rate 32 L/min for a-d, PVDF: PSF 1:1 wt/wt for b-d, fiber diameter 830 nm for a-b, fiber diameter 660 nm for d, areal density 1.12 mg/cm^2 for a and c-d, and acoustic regeneration at 100 Hz, 110 dB, 10 mins for a-h)

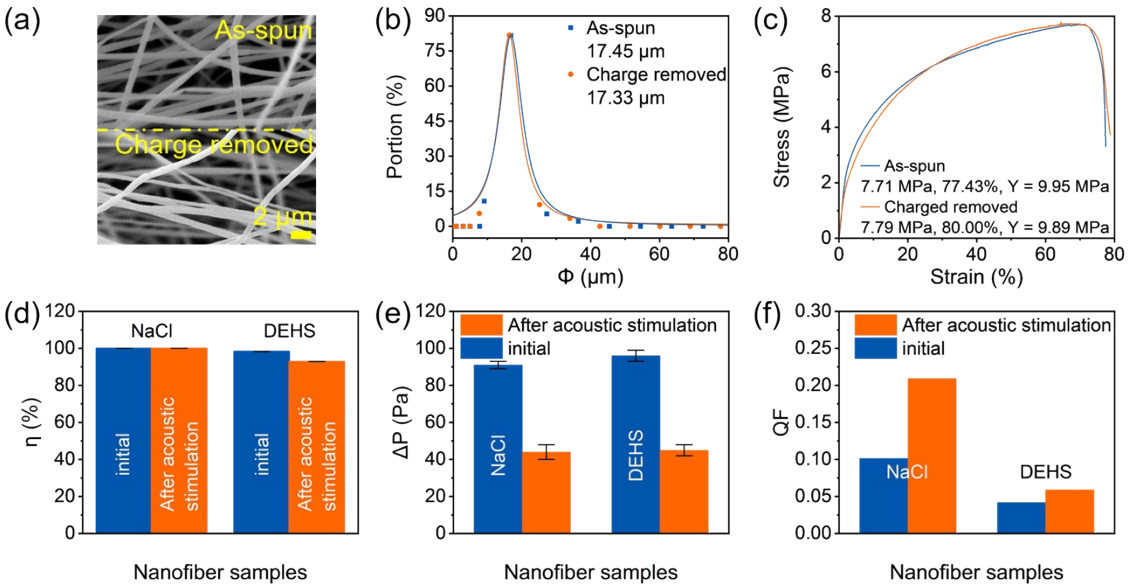

Figure S8. (a) SEM morphology, (b) pore size, and (c) mechanical properties of PVDF-PSF nanofiber membranes (PVDF: PSF 1:1, wt/wt) before and after electrostatic charge removal via IPA treatment. (d) η, (e) ΔP, and (f) QF of PVDF-PSF nanofiber membrane (50% PSF) in the spun state and after acoustic stimulation when filtering 0.3 μm NaCl and DEHS aerosol particles. (Airflow rate 32 L/min, PSF content 50%, fiber diameter 660 nm, areal density 1.12 mg/cm^2)

After 10 minutes of acoustic stimulation, the discharged membranes showed a reduction in ΔP of over 50% (from 96 Pa to 45 Pa), while the filtration efficiency for solid particles was restored to levels comparable to those of the pristine membranes.

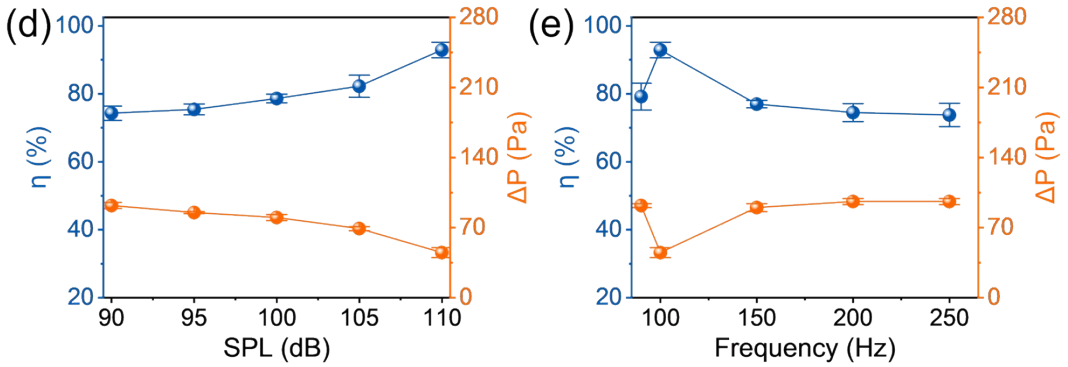

Figure S9. Effects of (d) SPL and (e) sound frequency on the oil $PM_{0.3}$ η and ΔP of ThePVDF-PSF nanofiber membranes. (Airflow rate 32 L/min, PVDF: PSF 1:1 wt/wt, fiber diameter 660 nm, areal density 1.12 mg/cm^2)

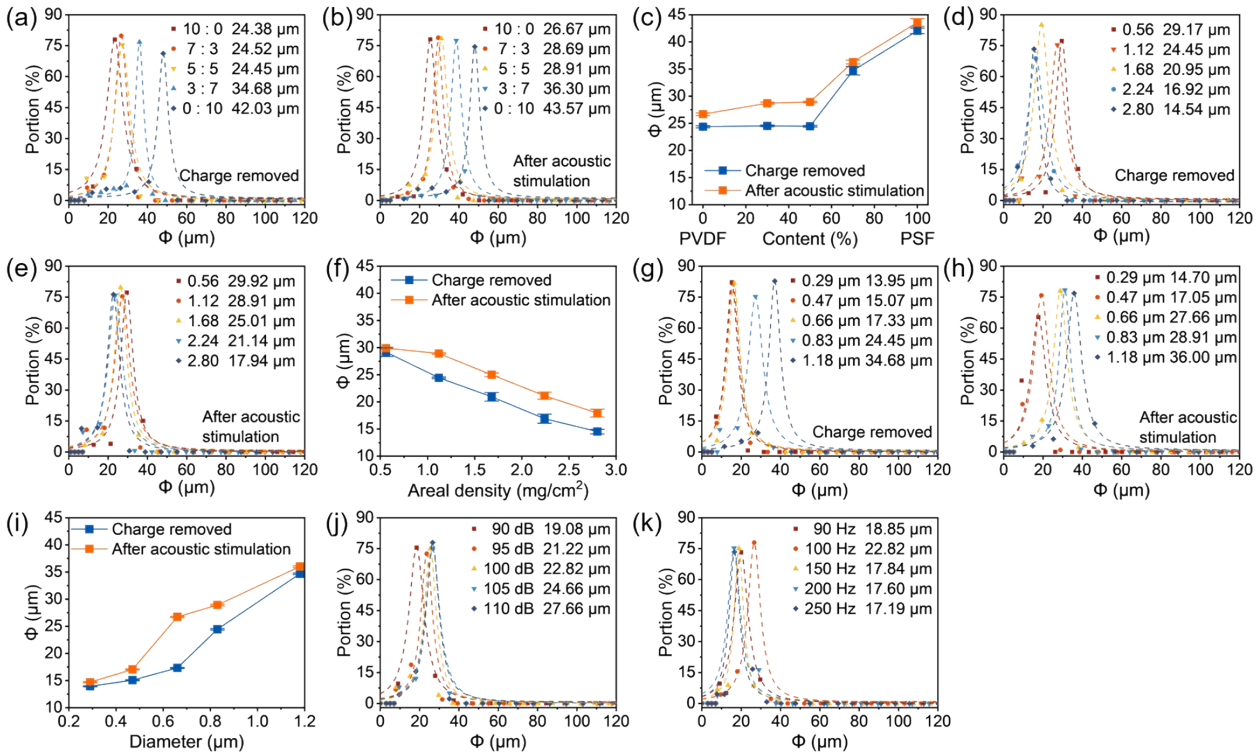

Figure S10. The pore size and distribution of the nanofiber membranes with different (a-c) PSF content, (d-f) areal density, and (g-i) nanofiber diameter before and after acoustic stimulation. Effects of (j) SPL (100 Hz) and (k) frequency (110 dB) on ϕ of the nanofiber membrane after acoustic stimulation. (PVDF: PSF 1:1 wt/wt for d-k, fiber diameter 830 nm for a-f, fiber diameter 660 nm for j-k, areal density 1.12 mg/cm^2 for a-c and g-k, and acoustic regeneration at 100 Hz, 110 dB, 10 mins for a-i)

Figure S10 illustrates the variation in Φ as a function of PSF content in charge-removed membranes. When the PSF content was below 50%, the average ϕ remained nearly constant at approximately 24.38 ± 0.21 μm, indicating minimal influence of polymer composition on pore structure within this range. However, as the PSF content increased from 50% to 100%, ϕ rose significantly from 24.44 ± 0.15 μm to 42.03 ± 0.51 μm, suggesting that higher PSF fractions lead to looser nanofiber packing. Acoustic stimulation induced a measurable expansion in ϕ across all compositions. For membranes containing 0–50% PSF, the pore size increased by 2.29–4.46 μm, whereas the increase was only 1.54 μm for pure PSF membranes. This reversible pore enlargement is attributed to sound-induced fiber vibration and electrostatic repulsion between adjacent fibers, which temporarily reorganizes the nanofiber network.

Φ decreased from 29.17 ± 0.82 μm to 14.54 ± 0.41 μm as the areal density increased from 0.56 to 2.80 mg/cm², reflecting a more compact membrane structure (Figure S10). After acoustic treatment, φ increased to 29.92 ± 0.18 μm and 17.94 ± 0.73 μm at the lowest and highest densities, respectively.

Fiber diameter also exerted a clear influence on pore structure (Figure S10). As the average diameter increased from 290 nm to 660 nm and 1.18 μm, ϕ values ranged from 13.95 ± 0.08 μm to 17.33 ± 0.08 μm and 34.68 ± 0.14 μm, consistent with trends reported in prior studies on nanofiber membranes. Acoustic stimulation induced modest pore expansion across all diameters, yielding post-stimulation ϕ values of 14.70 ± 0.11 μm (290 nm), 26.73 ± 0.12 μm (660 nm), and 36.01 ± 0.18 μm (1.18 μm).

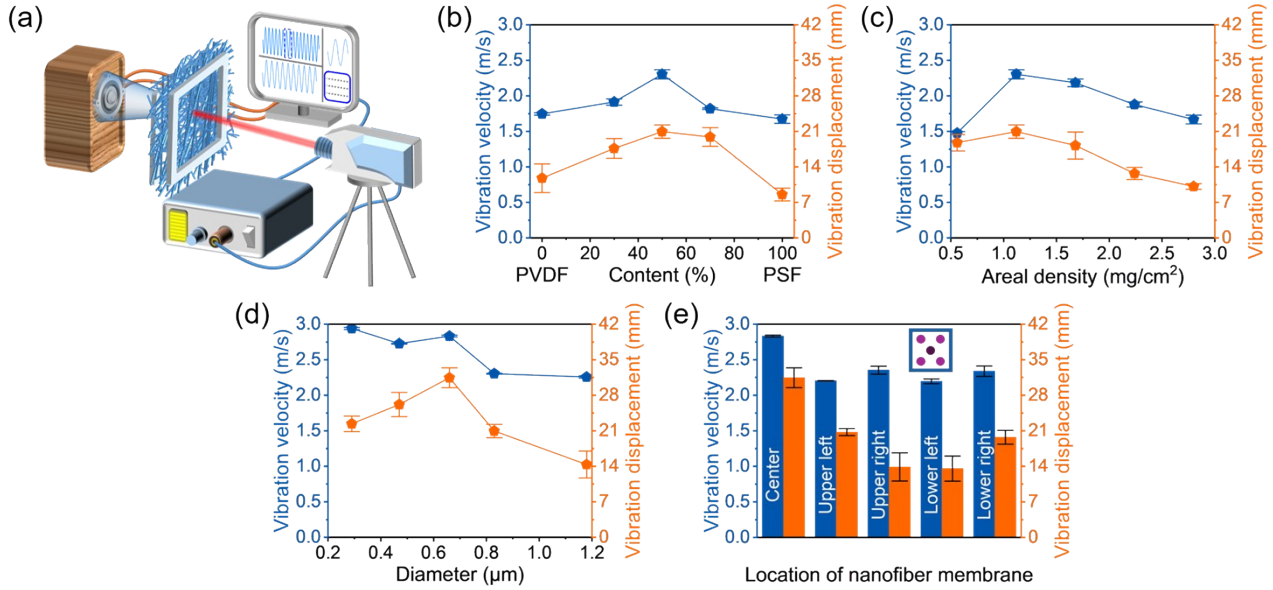

Figure S11. (a) Schematic diagram of vibration velocity and displacement test of nanofiber membranes. Effects of (b) PSF content, (c) areal density, and (d) fiber diameter on the vibration velocity of the nanofiber membranes. (e) The vibration velocity and displacement at different parts of the nanofiber membrane. (PVDF: PSF 1: wt/wt for b-e, fiber diameter 830 nm for b-c, fiber diameter 660 nm for e, areal density 1.12 mg/cm^2 for b and d-e, acoustic conditions 100 Hz, 110 dB for b-e)

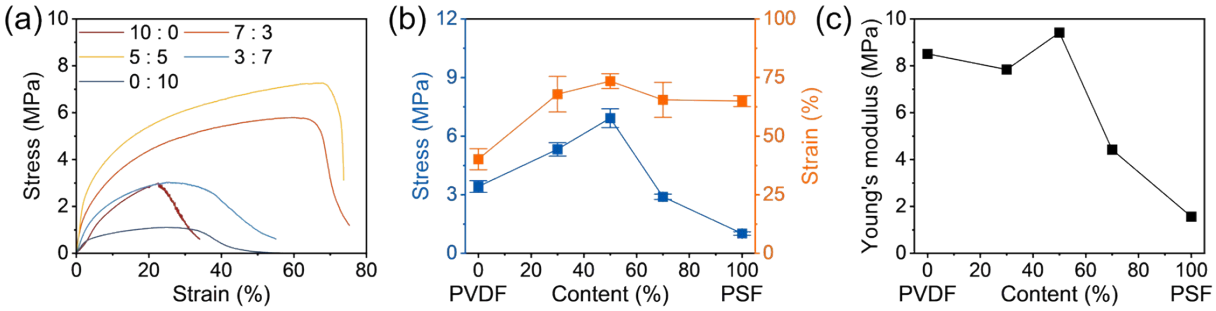

Figure S12. (a) Strain ~ stress curves with different PVDF: PSF weight ratios, b) tensile properties, and (c) Young's modulus of the nanofiber membranes with different PSF contents.

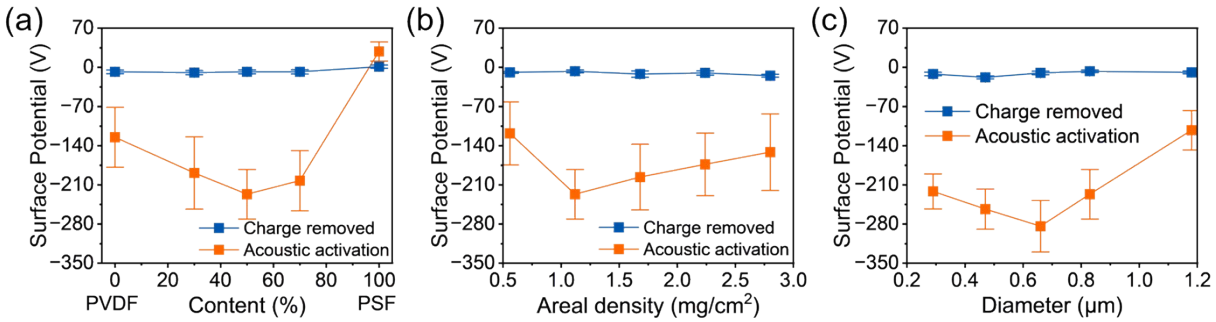

Figure S13. Effects of (a) PSF content, (b) areal density, and (c) fiber diameter on the surface potential of nanofiber membranes before and after acoustic stimulation. (Fiber diameter 830 nm for a-b; PVDF: PSF 1:1 wt/wt for b-c, areal density 1.12 mg/cm^2 for a and c, and acoustic condition 100 Hz, 110 dB, 10 min for a-c)

Fiber diameter influenced vibration and surface characteristics. Under 110 dB and 100 Hz stimulation, the 660 nm fiber membrane exhibited higher velocity and displacement than its counterparts (Figure S11). Increasing the fiber diameter from 290 nm to 660 nm increased the negative potential from –221.68 V to –283.9 V, whereas further increasing it to 1.18 μm reduced it to –112.4 V (Figure S13).

Membrane thickness, however, had a modest effect on vibration velocity and charge regeneration. Over an areal density range of 0.56–2.8 mg/cm², the vibration velocity varied between 1.4 and 2.3 m/s (Figure S11). Increasing the areal density from 0.56 mg/cm² to 2.8 mg/cm² resulted in an increase in surface potential from –118 V to –151.57 V (Figure S13).

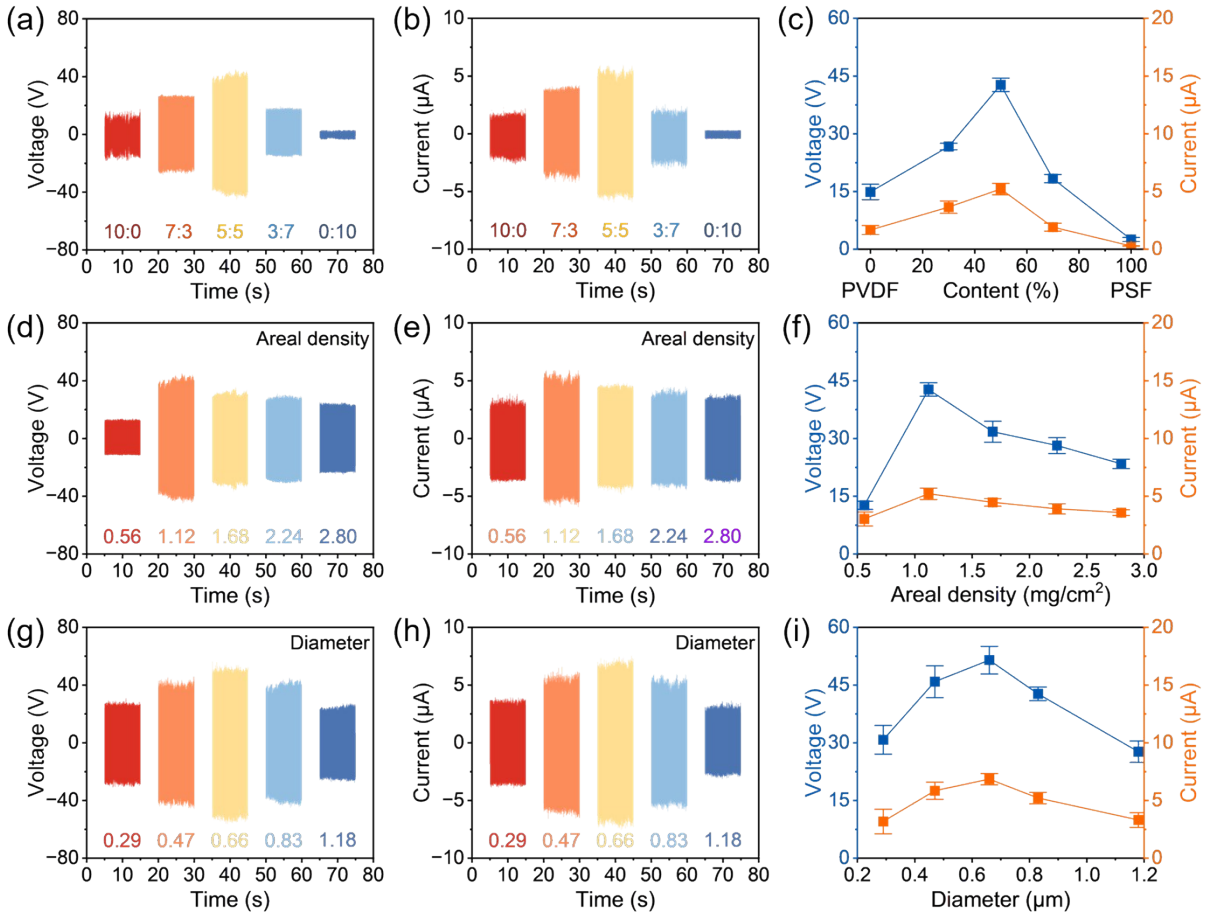

Figure S14. Effects of (a) PSF content, (b) areal density, and (c) fiber diameter on the voltage and current outputs of the nanofiber membranes. (Areal density 1.12 mg/cm² for a-c and g-i, PVDF: PSF 1:1 wt/wt, fiber diameter 830 nm for a-f, and acoustic condition 100 Hz, 110 dB for a-i)

Increasing areal density from 0.56 to 1.12 mg/cm² raised Voc from 12.66 ± 1.06 V to 42.72 ± 1.75 V and Isc from 3.04 ± 0.61 μA to 5.21 ± 0.49 μA, with further increases leading to diminished performance (Figure S13). Optimal fiber diameter was identified as 660 nm, yielding maximum outputs of Voc = 51.47 ± 3.59 V and Isc = 6.85 ± 0.49 μA, which declined to 27.67 ± 2.79 V and 3.31 ± 0.64 μA at 1.18 μm.

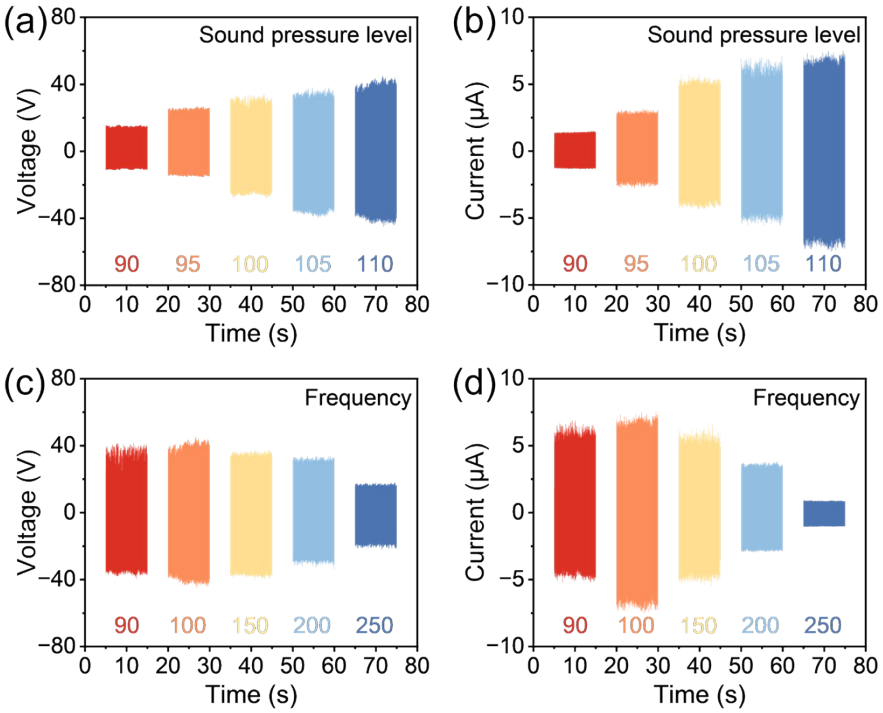

Figure S15. Effects of (a, b) SPL (100 Hz), and (c, d) frequency (110 dB) on the voltage and current outputs of PVDF-PSF nanofiber membrane. (PVDF: PSF 1:1 wt/wt, areal density 1.12 mg/cm^2, fiber diameter 660 nm)

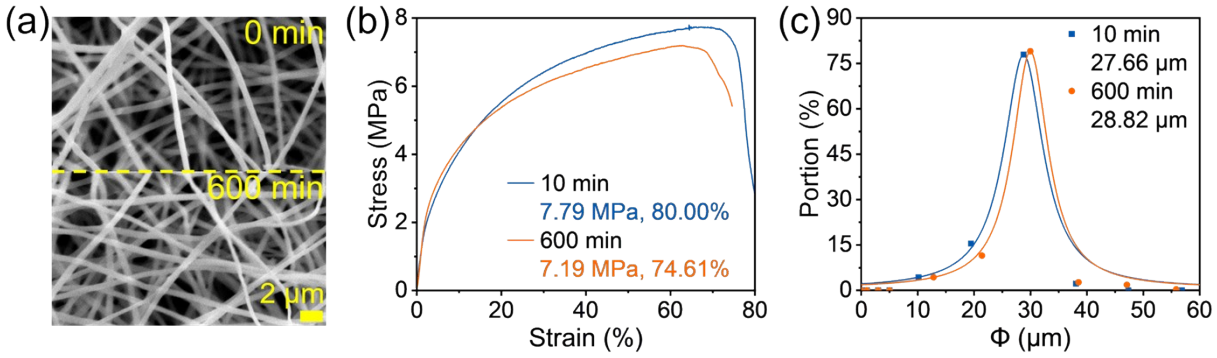

Figure S16. (a) SEM morphology, (b) mechanical properties, and (c) ϕ of the PVDF-PSF nanofiber membranes (1:1, wt/wt) before and after 10 h of continuous acoustic stimulation. (PVDF: PSF 1:1 wt/wt, areal density 1.12 mg/cm^2, fiber diameter 660 nm)

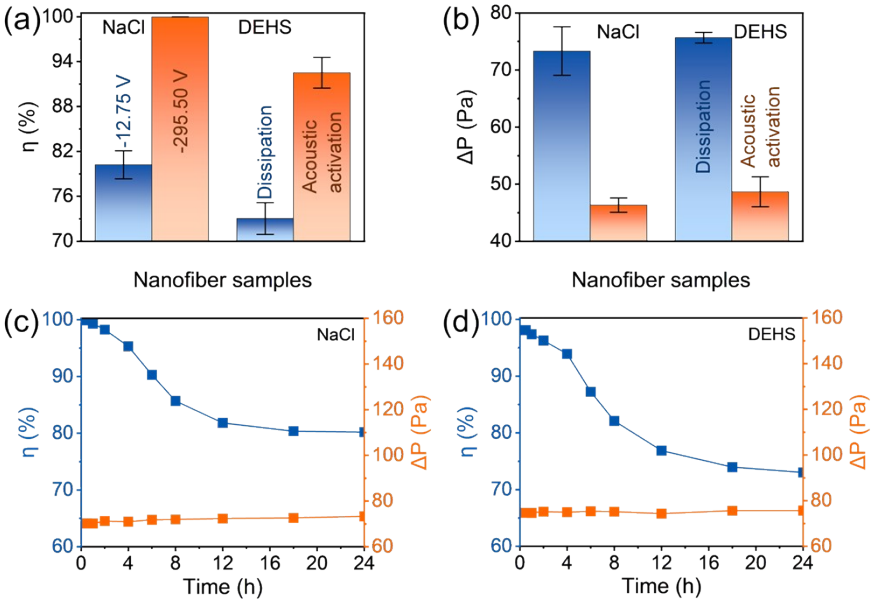

Figure 17. (a) η and (b) ΔP of PVDF-PSF nanofiber membranes after complete charge dissipation in a high-humidity environment (95% RH) and subsequent acoustic stimulation under 110 dB/100 Hz for 10 min. η and ΔP of PVDF-PSF nanofiber membranes for (c) $PM_{0.3}$ NaCl and (d) $PM_{0.3}$ DEHS particles during 24-hour exposure to 95% relative humidity at room temperature. (PVDF: PSF 1:1 wt/wt, areal density 1.12 mg/cm^2, fiber diameter 660 nm)

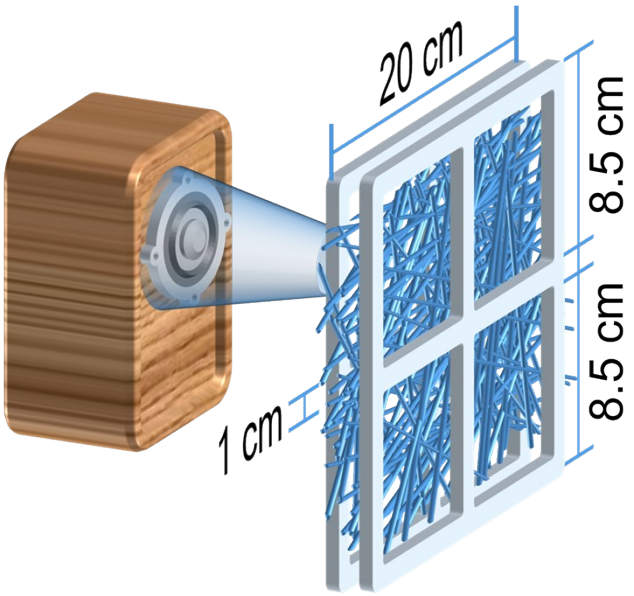

Figure S18. Schematic diagram of the acoustic stimulation regeneration filtration performance of nanofiber membranes.

SPL-Surface Potential Quantitative Correlation

Relationship between SPL and Vibration Velocity:

Under the plane wave approximation, the relationship between sound pressure p and medium particle vibration velocity *v* is expressed as:

$$P = \rho c v$$

where ρ is the air density (≈1.2 kg/m³), c is the speed of sound (≈340 m/s). The definition of sound pressure level Lp relative to sound pressure p is:

$$L_p = 20log_{10}\left(\frac{p}{p_0}\right)$$

Here, p_0=2×10⁻⁵ Pa (reference sound pressure). Combining the above two equations, the vibration velocity v can be directly expressed in terms of SPL:

$$v = \frac{p_0 10^{L_p/20}}{\rho c}$$

This equation indicates that vibration velocity increases monotonically with increasing SPL, which is consistent with experimental observations.

Vibrational Strain and Piezoelectric Surface Charge:

For piezoelectric phases (e.g., β-PVDF), the relationship between surface charge density and dynamic strain follows the piezoelectric effect:

$$\sigma_{piezo} = d_{33} Y \varepsilon$$

where d_{33} is the piezoelectric coefficient, Y is the Young's modulus, and ε is the dynamic strain induced by vibration (related to fiber vibration displacement δ and fiber dimensions). If the vibration is harmonic ($\varepsilon_t = \varepsilon_0 sin(2\pi f t)$, where f is the vibration frequency), the change in surface potential contributed by the piezoelectric effect (ΔV_{piezo}) can be approximately expressed as:

$$\Delta V_{piezo} \propto \frac{\sigma_{piezo} t}{\varepsilon_0 \varepsilon_r}$$

Here, t is the equivalent thickness of the dielectric layer, ε_0 is the vacuum permittivity, and ε_r is the relative permittivity of the material.

Vibration and Triboelectric Surface Charge:

The triboelectric surface charge density σ_{tribo} is closely related to contact-separation behavior, described by the semi-empirical relationship:

$$\sigma_{tribo} \propto v^{\alpha} f^{\beta}$$

where μ is the triboelectric coefficient, v is the relative sliding/separation velocity between fibers (positively correlated with vibration velocity), N is vibration frequency f, and α and β are experimentally fitted exponents (typically close to 1).

Comprehensive Relationship between Surface Potential and SPL

Assuming the charge contributions from piezoelectric and triboelectric effects are linearly superposed, the total surface potential V_s can be written as:

$$V_s \approx k_1 \sigma_{piezo} + k_2 \sigma_{tribo}$$

where k_1 and k_2 are charge-to-potential conversion coefficients. Substituting the aforementioned correlations between SPL, vibration velocity, strain, and charge density, an approximate power-law relationship between V_s and L_p is derived:

$$V_s \propto 10^{L_P/20} \text{ or } V_s = A(10^{\frac{L_P}{20}})^{\gamma} + B$$

Fitting to the experimental data yields the parameters: A = −0.047, γ = 0.681, B = −21.488, with a goodness-of-fit R^2 = 0.99, indicating excellent agreement between the model and the experimental

results.

Energy Efficiency Calculation Metric

To quantitatively compare the energy efficiency of acoustic and contact-based mechanical regeneration, we defined a dedicated metric, $\bar{E}$ (%/J), that represents the filtration efficiency increment ($\Delta\eta$) per unit of total energy consumed during regeneration. The calculation formula is as follows:

$$\bar{E} = \frac{\Delta\eta}{E_{total}}$$

where $E_{total} = P \times t$ (E_{total} is total energy, P is operating power, t is regeneration time).

A higher $\bar{E}$ value indicates superior energy efficiency in restoring the filtration performance of charge-depleted membranes. For the acoustic regeneration method, the filtration efficiency increment reached 24.85% at an operating power of 100 W, yielding a $\bar{E}$ of 1.49 %/J; in contrast, the contact-based mechanical regeneration method achieved a filtration efficiency increment of 24.55% at an operating power of 160 W, with a corresponding $\bar{E}$ of only 0.92 %/J.

Table S1. Filtration performance of the nanofiber membranes after charge removal

PVDF: PSF	Solid $PM_{0.3}$			Oil $PM_{0.3}$		
Weight ratios[a]	η (%)	ΔP (Pa)	QF (Pa^{-1})	η (%)	ΔP (Pa)	QF (Pa^{-1})
10 : 0	71.00	60	0.021	59.05	62	0.014
7 : 3	70.57	61	0.020	60.50	62	0.015
5 : 5	71.89	61	0.021	60.00	61	0.015
3 : 7	54.19	37	0.021	45.95	40	0.015
0 : 10	30.24	18	0.020	26.10	22	0.014

a. fiber diameter≈830 nm, areal density=1.12 mg/cm^2, flowrate=32 L/min.

Table S2. Filtration performance of the nanofiber membranes after sound stimulation

PVDF: PSF	Solid $PM_{0.3}$			Oil $PM_{0.3}$		
Weight ratios[a]	η (%)	ΔP (Pa)	QF (Pa^{-1})	η (%)	ΔP (Pa)	QF (Pa^{-1})
10 : 0	78.97	50	0.031	63.00	51	0.020
7 : 3	83.73	47	0.039	64.65	50	0.021
5 : 5	91.89	35	0.072	74.60	38	0.036
3 : 7	69.06	28	0.042	55.95	32	0.026
0 : 10	31.22	17	0.022	26.80	17	0.018

a. fiber diameter≈830 nm, areal density=1.12 mg/cm^2, flowrate=32 L/min, after 110 dB/100 Hz acoustic simulation for 10 min.

Table S3. Comparison with other filter materials reported for oil aerosol filtration

Samples	Salt particles η (%)	ΔP for salt particles (Pa)	Oil mist η (%)	ΔP for oil mist (Pa)	Refs
PAN/FPU nanofiber	99.6	82	92.5	100	S1
PAN/PAN-FPU nanofiber	99.84	163.7	99.88	168	S2
PP nonwoven fabric	99.84	94.56	99.16	94.49	S3
Bead-on-string PAN nanofiber	99.3	27	99.3	27	S4
PP/magnesium stearate nonwoven fabric	99.03	82.32	97.96	84.28	S5
PVA-PAA-SiO_2-Ag NP nanofiber	78.17	57	78.8	55	S6
PP-PS nonwoven fabric	63.1	67.4	86.5	67.4	S7
PLA nonwoven fabric	98.6	122	95.4	145	S8
PAN/PAMAM/TEO nanofiber	92.8	89.2	80.1	89.2	S9
PLA/CTAB nanofiber	98.38	156	92.4	162	S10
PCL nanofiber	99.91	132	99.97	125	S11
F-MOF@PEI/PVDF-HFP/FAS nanofiber	99.95	152	99.55	147	S12
Cellulose fibers	99.45	45.7	98.49	45.7	S13
Nylon/FS-60	85	78	97.2	126	S14
PVDF/PSF nanofiber[a]	99.99	44	92.90	45	this work
PVDF/PSF nanofiber[b]	99.99	117	99.67	125	this work

a. PVDF: PSF 1:1 wt/wt, diameter 660 nm, areal density 1.12 mg/cm^2, after 110 dB/100 Hz acoustic simulation for 10 min; b. PVDF: PSF 1:1 wt/wt, diameter 830 nm, areal density 2.80 mg/cm^2, after 110 dB/100 Hz acoustic simulation for 10 min.

Table S4. Quantitative comparison of filtration performance metrics between PVDF-PSF nanofiber membranes subjected to acoustic mechanical regeneration

Performances	Acoustic Stimulation[a]	Mechanical Stimulation[b]
NaCl $PM_{0.3}$ η (%)	75.14→99.99	75.26→99.81
DEHS $PM_{0.3}$ η (%)	73.70→92.90	65.50→84.30
ΔP (Pa)	96 Pa→45 Pa	No change
Surface Potential (V)	-283.9	-181.89
Young's Modulus Reduction after 30 Cycles (%)	4.12	6.19
NaCl $PM_{0.3}$ η after 30 Cycles (%)	99.99	98.13
NaCl $PM_{0.3}$ η Decay after 30 Cycles (%)	No decay	1.9%
Energy Consumption per Unit Efficiency Improvement (%/J)	1.49	0.92

a. PVDF: PSF 1:1 wt/wt, diameter 660 nm, areal density 1.12 mg/cm^2, after 110 dB/100 Hz acoustic simulation for 10 min; b. PVDF: PSF 1:1 wt/wt, diameter 660 nm, areal density 1.12 mg/cm^2, after 15 N/1 Hz mechanical simulation for 10 min.

REFERENCES

S1. J. Xiong, W. Shao, L. Wang, C. Cui, Y. Jin, H. Yu, P. Han, Y. Gao, F. Liu, Q. Ni and J. He, *Macromol. Mater. Eng.*, 2021, **306**.

S2. H. Zhang, S. Fang, Z. Wu, S. R. Islam and X. Qin, *ACS Appl. Nano Mater.*, 2023, **6**, 7619-7628.

S3. X. Zhang, Y. Wang, R. Ni, H. Zhang, J. Liu, Y. Zhao and X. Jin, *Sep. Purif. Technol.*, 2022, **303**.

S4. J. J. Huang, Y. Tian, R. Wang, M. Tian and Y. Liao, *Sep. Purif. Technol.*, 2020, **237**.

S5. X. Zhang, J. Liu, H. Zhang, J. Hou, Y. Wang, C. Deng, C. Huang and X. Jin, *Polymers*, 2021, **13**.

S6. M. Zhu, D. Hua, H. Pan, F. Wang, B. Manshian, S. J. Soenen, R. Xiong and C. Huang, *J. Colloid Interface Sci.*, 2018, **511**, 411-423.

S7. S. Jung, J. An, H. Na and J. Kim, *Polymers*, 2019, **11**.

S8. Y. Zhang, J. Wang, S. Yuan, M. Hussain, X. Ye, Y. Fang, B. Yu and F. Zhu, *Ind. Eng. Chem. Res.*, 2024, **63**, 13230-13237.

S9. M. Mounesan, S. Akbari and B. E. Brycki, *J. Ind. Text.*, 2021, **51**, 6333S-6352S.

S10. Y.-H. Yu, Y. Huang, J.-F. Zhang, W.-T. Lin, W.-L. Li, X.-Y. Ye, J. Ji, Z.-K. Xu and L.-S. Wan, *ACS Appl. Polym. Mater.*, 2023, **5**, 10426-10437.

S11. H. Liu, J. Shi, Y. Liang, S. Zhou, Y. Liu, Y. Liu, X. Chen and D. Yu, *Advanced Materials*, 2025, DOI: 10.1002/adma.202419143, e2419143.

S12. X. Zhang, Y. Zhang, H. Xun, Y. Xu, L. Zhang, J. Fang, H. Niu and H. Zhou, *Sep. Purif. Technol.*, 2025, **362**.

S13. J. Nie, B. Sun, T. Jiao, J. Liao, M. Zhang, R. Yang and Y. Li, *J. Hazard. Mater.*, 2025, **489**, 137557.

S14. H. Zhou, H. Niu, H. Wang, W. Yang, X. Wei, H. Shao and T. Lin, *Nanoscale*, 2020, **12**, 2359-2365.